PLANE-STRAIN CRACK-TIP FIELDS FOR POWER-LAW HARDENING ORTHOTROPIC MATERIALS

Jwo PAN

Department of Mechanical Engineering and Applied Mechanics, The University of Michigan, Ann Arbor, MI 48109, U.S.A.

C. Fong SHIH

Division of Engineering Brown University Providence, RI 02912, U.S.A.

Near-tip stress and strain fields for power-law hardening orthotropic materials under plane-strain conditions are presented. Plastic orthotropy is described by Hill's quadratic yield function. The angular variations of these HRR-type fields depend on a single parameter which specifies the state of plastic orthotropy. Near-tip fields for highly orthotropic materials differ substantially from the fields for isotropic materials. Mode I (symmetric) and mode II (anti-symmetric) solutions for different degrees of plastic orthotropy are given. The angular stress distributions for the low-hardening material agree remarkably well with the plane-strain slip-line fields. Based on the singularity fields, effective stress contours are constructed. The applicability of these fields in the context of a fiber-reinforced composite containing a macroscopic flaw is discussed.

1. Introduction

Plastic anisotropy in crystalline materials arises from preferred crystallographic orientation of grains and/or the development of texture due to prior plastic deformation. Composite materials may be treated as macroscopically homogeneous but anisotropic if the characteristic size of the fiber, such as the fiber diameter as well as fiber spacing, is small compared with the relevant macroscopic dimension of the composite system e.g., the plastic zone size, physical dimensions of the component, and other characteristic macroscopic lengths.

A phenomenological plasticity theory for orthotropic material has been proposed by Hill (1948). The yield function is a quadratic function of the stresses. In a later study Hill (1979) suggests non-quadratic yield functions to account for the so-called anomalous behavior of some materials.

In this study we adopt the simpler quadratic yield function in conjunction with power-law hardening as descriptive of the orthotropic plastic behavior at 'large' plastic strains in the vicinity of

a stationary crack tip. Deformation-induced finite geometry changes associated with blunting at the crack tip are neglected in the formulation of the equations governing plane-strain deformation. A systematic examination of the effect of plastic anisotropy on Mode I and Mode II singular crack-tip fields is carried out. The size and shape of effective stress contours are also shown. Stress fields for perfectly plastic materials are discussed. Singular crack-tip fields for orthotropic power-law hardening solids have been discussed by Hayashi (1979); however the angular variation of the fields was detailed for mildly orthotropic materials, and only for the case of plane stress.

Strain hardening and non-hardening plasticity solutions which elucidate the behavior at the tip of a stationary crack in an isotropic material have been obtained by Hutchinson (1968a,b) and Rice and Rosengren (1968). The amplitude of the HRR singularity fields is given by the path-independent J-integral (Rice, 1968a). To the extent that the singularity fields dominate over a region which is larger than the fracture process zone, the onset of fracture and possibly limited amounts of crack

growth can be phrased in terms of the attainment of a critical value of J and the J-resistance curve. These developments, including an excellent discussion of the conditions which validate the J-based nonlinear fracture mechanics methodology, can be found in the review article by Hutchinson (1983).

2. Orthotropic plasticity

We consider the case where the pronounced preferred crystallographic orientation is already firmly established and restrict the discussion to a range of plastic straining such that further changes in crystallographic orientation is negligible. With these assumptions the state of plastic orthotropy remains constant and is specified by the initial value of the tensile yield stresses in the three principal directions of orthotropy and the three yield stresses in shear with respect to the principal axes of orthotropy. Since the state of plastic orthotropy is unchanging, the hardening behavior is completely described by a single tensile (or shear) stress versus plastic strain curve. We choose the axes of the orthogonal Cartesian coordinate system x_1, x_2, x_3 to be coincident with the axes of orthotropic symmetry X_1, X_2, X_3. Hill's (1948) yield criterion can be written in the form

$$\phi(\sigma_{ij}) \equiv F(\sigma_{22} - \sigma_{33})^2 + G(\sigma_{33} - \sigma_{11})^2$$
$$+ H(\sigma_{11} - \sigma_{22})^2$$
$$+ 2L\sigma_{23}^2 + 2M\sigma_{31}^2 + 2N\sigma_{12}^2 = Q^2 \quad (2.1)$$

where $\phi(\sigma_{ij})$ represents the current yield surface in stress space, and F, G, H, L, M and N are dimensionless constants which describe the state of plastic orthotropy. Without loss of generality, an effective yield strength parameter Q can be defined to represent the characteristic size of the elastic domain at the current stress state. The characteristic stress Q can be taken to depend upon the plastic work W^p. If ϕ is also the plastic potential, the increment of the plastic strain, $d\epsilon_{ij}^p$, is determined to within a constant of proportionality (Hill, 1950). Then Q can be made to depend upon $\int d\epsilon_e^p$ where the definition for the increment

of the effective plastic strain, $d\epsilon_e^p$, follows from the statement that $dW^p = \sigma_{ij} d\epsilon_{ij}^p = Q d\epsilon_e^p/\sqrt{3}$ (the factor $\sqrt{3}$ arises in deference to the isotropic plasticity convention and the identification of Q as the shear stress parameter as defined below).

Let X_0, Y_0 and Z_0 be the initial yield stresses along the axes of orthotropic symmetry and R_0, S_0, T_0 be the corresponding shear yield stresses. With no loss of generality, and for reasons that will become clear in the later sections where the plane strain analysis is discussed, we identify Q with the shear yield stress T. With this normalization, these relations follow (Hill, 1948, 1950).

$$G + H = (T_0/X_0)^2, \qquad H + F = (T_0/Y_0)^2,$$
$$F + G = (T_0/Z_0)^2, \qquad 2L = (T_0/R_0)^2,$$
$$2M = (T_0/S_0)^2, \qquad 2N = 1. \quad (2.2)$$

We introduce generalized effective 'shear' and 'tensile' yield stresses defined by

$$\tau_e^2 = \tfrac{1}{3}\sigma_e^2 = F(\sigma_{22} - \sigma_{33})^2 + G(\sigma_{33} - \sigma_{11})^2$$
$$+ H(\sigma_{11} - \sigma_{22})^2 + L(\sigma_{23}^2 + \sigma_{32}^2)$$
$$+ M(\sigma_{31}^2 + \sigma_{13}^2) + N(\sigma_{12}^2 + \sigma_{21}^2). \quad (2.3)$$

For clarity of manipulations all nine stresses are distinguished in (2.3) and are regarded as distinct (independent) variables. The yield criterion (2.1) can be restated as

$$\tau_e = \sigma_e/\sqrt{3} = T(W^p) \quad (2.4)$$

and the stress S_{ij} directed along the normal to the yield surface is given by

$$S_{ij} = \partial\phi/\partial\sigma_{ij} = \partial\tau_e^2/\partial\sigma_{ij}. \quad (2.5)$$

Most plasticity analyses of near-tip behavior employ stress-strain characterization taken from a Ramberg-Osgood uniaxial stress-strain relation. For our analysis, a more convenient form is the Ramberg-Osgood shear strain-shear stress relation

$$\gamma/\gamma_0 = \tau/\tau_0 + \alpha(\tau/\tau_0)^n \quad (2.6)$$

where n is the strain hardening exponent, α is a material constant, τ_0 is a reference shear stress and $\gamma_0 = \tau_0/G$ is the associated reference strain

with G being a representative shear modulus. We use (2.3) and (2.5) to generalize the relation between the shear stress and the plastic strain (2.6) to multiaxial states in a manner that will be useful for subsequent development. The resulting deformation theory relation between the plastic strains and the stresses is

$$\frac{\epsilon_{ij}^{P}}{\gamma_0} = \frac{1}{2}\alpha\left(\frac{\tau_e}{\tau_0}\right)^{n-1}\frac{S_{ij}}{\tau_0}. \tag{2.7}$$

Since γ and τ in (2.6) are the shear strain and stress with respect to the X_1- and X_2-axes (2.7) can be restated as

$$\frac{\epsilon_{ij}^{P}}{\gamma_0} = \frac{1}{2}\alpha\left(\frac{\tau_e}{T_0}\right)^{n-1}\frac{S_{ij}}{T_0} \tag{2.8}$$

where $\gamma_0 = T_0/G$ and α is the material constant particular to the present stress-strain curve. Relation (2.8) together with the dimensionless constants F, G, H, L, M and N defined by (2.2) describe the plastic behavior of the material.

Some comments are in order. As implied by the yield function (2.1) (and the plastic potential), plastic strains are volume preserving, hence $S_{ii} = 0$ (see (2.7)). In this sense S_{ij} may be thought of as the generalized deviatoric stress. If the material is isotropic then $F = G = H = \frac{1}{6}$ and $L = M = N = \frac{1}{2}$, and (2.3) and (2.7) reduce to the standard J_2 deformation theory relations with S_{ij} (2.5) being the deviatoric stress

3. Plane-strain specialization

We suppose that elastic strains are negligible compared to plastic strains (this is certainly the case in the immediate vicinity of the crack tip). Invoking plane-strain condition then leads to the relation

$$\sigma_{33} = (G\sigma_{11} + F\sigma_{22})/(G + F). \tag{3.1}$$

Using (3.1) in (2.3) and requiring that $\sigma_{23} = \sigma_{31} = 0$, we have

$$\tau_e^2 = \frac{1}{4}p(\sigma_{11} - \sigma_{22})^2 + \sigma_{12}^2 \tag{3.2}$$

where

$$\frac{1}{4}p = FG/(F + G) + H. \tag{3.3}$$

Furthermore

$$S_{11} = \frac{1}{2}p(\sigma_{11} - \sigma_{22}), \qquad S_{22} = \frac{1}{2}p(\sigma_{22} - \sigma_{11}),$$
$$S_{12} = \sigma_{12} \tag{3.4}$$

and S_{33} vanishes identically. The plastic strain-stress relations are given by

$$\epsilon_{11}^{P}/\gamma_0 = \frac{1}{2}\alpha(\tau_e/\tau_0)^{n-1}S_{11}/\tau_0,$$
$$\frac{\epsilon_{12}^{P}}{\gamma_0} = \frac{1}{2}\alpha(\tau_e/\tau_0)^{n-1}S_{12}/\tau_0 \tag{3.5}$$

with $\epsilon_{11}^{P} = -\epsilon_{22}^{P}$, and $\epsilon_{33}^{P} = 0$.

We emphasize that the simple forms for (3.1), (3.2), and (3.4) only hold when the principal axes of orthotropy X_1, X_2, X_3 coincide with the axes of reference x_1, x_2, x_3 and the plane of plastic flow is normal to x_3 (and X_3). If the X_1-axis is arbitrarily inclined from the x_1-axis (x_3 and X_3 are still coincident) then the expressions for τ_e and S_{ij} can be found by transforming the stress components. Let the X_1-axis be rotated (counter-clockwise) by an angle ψ from the x_1-axis. Applying the standard transformations we get

$$\tau_e^2 = \frac{1}{4}p\left[(\sigma_{11} - \sigma_{22})\cos 2\psi - 2\sigma_{12}\sin 2\psi\right]^2$$
$$+ \frac{1}{4}\left[(\sigma_{11} - \sigma_{22})\sin 2\psi + 2\sigma_{12}\cos 2\psi\right]^2. \tag{3.6}$$

A similar expression can be written for σ_{33}. The stresses S_{ij} obtained by substituting (3.6) in (2.5) and carrying out the partial differentiation (the term $2\sigma_{12}$ in (3.6) must be treated as two distinct independent variables $\sigma_{12} + \sigma_{21}$ in the differentiation) are,

$$S_{11} = -S_{22} = \frac{1}{2}(\sigma_{11} - \sigma_{22})(p\cos^2 2\psi + \sin^2 2\psi)$$
$$- \sigma_{12}(p - 1)\cos 2\psi\sin 2\psi. \tag{3.7}$$

$$S_{12} = -\frac{1}{2}(\sigma_{11} - \sigma_{22})(p - 1)\cos 2\psi\sin 2\psi$$
$$+ \sigma_{12}(p\sin^2 2\psi + \cos^2 2\psi).$$

For $p = 1$, (3.6) and (3.7) reduce to the usual definitions for shear effective stress and deviatoric stress.

Suppose $\psi = \frac{1}{2}m\pi$ $(m = 1, 2, 3)$. For these particular orientations of the axes of orthotropy, (3.6) and (3.7) are identical to (3.2) and (3.4) respectively. Suppose $\psi = \frac{1}{4}\pi + \frac{1}{2}m\pi$ $(m = 0, 1, 2, 3)$ then we have

$$\tau_c^2 = \frac{1}{4}(\sigma_{11} - \sigma_{22})^2 + p\sigma_{12}^2, \tag{3.8}$$

$$S_{11} = \frac{1}{2}(\sigma_{11} - \sigma_{22}), \qquad S_{22} = \frac{1}{2}(\sigma_{22} - \sigma_{11}),$$

$$S_{12} = p\sigma_{12}. \tag{3.9}$$

The preceeding results together with the plastic strain–stress relations given by (2.7) demonstrate that under plane-strain conditions (X_3-axis normal to planes of plastic flow) the axes of orthotropy as well as axes inclined at $\frac{1}{4}\pi + \frac{1}{2}m\pi$ $(m = 0, 1, 2, 3)$ to the X_1-axis are axes of symmetry. It is also evident that the state of plastic orthotropy is specified by the single parameter p (see (3.2) and (3.8)). The connection between the forms (3.2) and (3.8) will be made in Section 7.

If the material is isotropic, $p = 1$. We also note that various values of F, G and H can result in $p = 1$. For example, if the material is rotationally symmetrical about the x_3-axis so that $F + 2H = G + 2H = \frac{1}{2}$ $(F \neq H)$, then $p = 1$. We emphasize that with $p = 1$, (3.2), (3.4), (3.8) and (3.9) dictate isotropic plastic flow. It is obvious from (3.3) that a given value of p (including $p = 1$) can be attained by different values of F, G and H. Nevertheless the state of plane-strain plastic orthotropy is specified by the single parameter p. As the value of p deviates from unity, the plastic response of the material becomes increasingly anisotropic. The plane-strain plastic behavior of an orthotropic material which is weak in shear (compared to the tensile/compressive yield stress) is characterized by $p < 1$. A material with high shear yield stress is characterized by $p > 1$. These aspects are elaborated upon in Sections 5 and 7. Hill (1950) has noted that p and T can be experimentally determined by two compression tests (under conditions of plane strain) at $0°$ and $45°$ to the axes of orthotropy; this can be easily deduced by using (2.4) with (3.2) and (3.8). When it is required to calculate σ_{33} all four parameters F, G, H and N (or X_0, Y_0, Z_0, T_0) must be known.

4. Dominant singularity analysis

We consider the planar crack problem as depicted in Fig. 1, where the rectangular Cartesian coordinates x_1 and x_2 are centered at the crack tip, and x_3 is perpendicular to the $x_1 - x_2$ plane. In this section and in Sections 5 and 6 we will confine the discussion to the case where the axes of reference coincide with symmetry axes of orthotropy (i.e. $\psi = 0$). The polar coordinates in the $x_1 - x_2$ plane are shown in Fig. 1.

The arguments leading to the HRR singularity fields have been detailed by Hutchinson (1968a, b), Rice and Rosengren (1968) for pure-mode fields, and by Shih (1974) for mixed-mode fields. In exactly the same fashion, application of the J-integral (Rice, 1968a) to the present boundary value problem shows that the dominant singularity governing the asymptotic behavior of the stresses, strains and displacements can be written as

$$\sigma_{ij} = \sigma_0 \left[\frac{J}{\alpha\sigma_0\epsilon_0 Ir} \right]^{1/(n+1)} \tilde{\sigma}_{ij}(\theta; n, p, M),$$

$$\epsilon_{ij}^{p} = \alpha\epsilon_0 \left[\frac{J}{\alpha\sigma_0\epsilon_0 Ir} \right]^{n/(n+1)} \tilde{\epsilon}_{ij}(\theta; n, p, M), \tag{4.1}$$

$$u_i - \hat{u}_i = \alpha\epsilon_0 r \left[\frac{J}{\alpha\sigma_0\epsilon_0 Ir} \right]^{n/(n+1)} \tilde{u}_i(\theta; n, p, M).$$

Written in the above form, the fields reduce precisely to the HRR singularity fields for $p = 1$ (Hutchinson, 1983). For all values of p, σ_0, and ϵ_0 in (4.1) are identified with the material parameters in (2.8) through the relations $\sigma_0 = \sqrt{3}\,\tau_0$ ($\tau_0 \equiv T_0$) and $\epsilon_0 = \gamma_0/\sqrt{3}$. Thus all material parameters in (4.1) including α and n are defined by the plastic shear strain–shear stress relation (2.8) while the plane-strain plastic orthotropy parameter p is defined by (3.3). The (plane-strain) dimensionless constant I and the θ-variations of the (plane-strain) dimensionless functions $\tilde{\sigma}_{ij}$, $\tilde{\epsilon}_{ij}$ and $\tilde{u}_i$ depend on the strain hardening exponent n, on the state of plastic orthotropy p, and on the mode parameter M (Mode I or II or mixed mode); the constants $\hat{u}_i$ allow for a possible translation of the crack tip itself. The angular functions are normalized by setting the maximum value of the θ-variation of $\tilde{\sigma}_e$ to unity (or equivalently the maximum
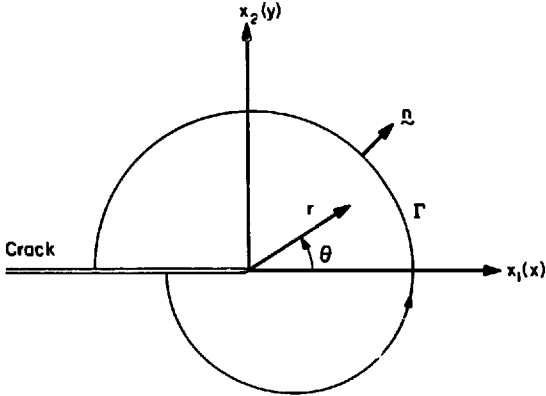
Fig. 1. Conventions at crack tip.

value of the effective shear stress, $\tilde{\tau}_e$, to $1/\sqrt{3}$). With this normalization the present angular functions for $p = 1$ are exactly the functions given by Hutchinson (1968a, b) and Shih (1974, 1983) for isotropic plasticity. For completeness we list these relations

$$\tilde{\tau}_e^2 = \tfrac{1}{3}\tilde{\sigma}_e^2$$

$$= \tfrac{1}{4}p\left[(\tilde{\sigma}_{rr} - \tilde{\sigma}_{\theta\theta})\cos 2\theta - 2\tilde{\sigma}_{r\theta}\sin 2\theta\right]^2$$

$$+ \tfrac{1}{4}\left[(\tilde{\sigma}_{rr} - \tilde{\sigma}_{\theta\theta})\sin 2\theta + 2\tilde{\sigma}_{r\theta}\cos 2\theta\right]^2, \quad (4.2)$$

$$\tilde{S}_{rr} = \frac{\partial \tilde{\tau}_e^2}{\partial \tilde{\sigma}_{rr}}, \qquad \tilde{S}_{\theta\theta} = \frac{\partial \tilde{\tau}_e^2}{\partial \tilde{\sigma}_{\theta\theta}}, \qquad \tilde{S}_{r\theta} = \tfrac{1}{2}\frac{\partial \tilde{\tau}_e^2}{\partial \tilde{\sigma}_{r\theta}},$$
$$(4.3)$$

$$\tilde{\epsilon}_{rr} = -\tilde{\epsilon}_{\theta\theta} = \tfrac{3}{2}\tilde{\sigma}_e^{n-1}\tilde{S}_{rr}, \qquad \tilde{\epsilon}_{r\theta} = \tfrac{3}{2}\tilde{\sigma}_e^{n-1}\tilde{S}_{r\theta}, \quad (4.4)$$

$$I = \int_{-\pi}^{\pi}\left\{\frac{n}{n+1}\tilde{\sigma}_e^{n+1}\cos\theta\right.$$

$$- \left[\sin\theta\left(\tilde{\sigma}_{rr}(\tilde{u}_\theta - \tilde{u}_r^{\cdot}) - \tilde{\sigma}_{r\theta}(\tilde{u}_r + \tilde{u}_\theta^{\cdot})\right)\right.$$

$$+ \left.\left.\frac{1}{n+1}(\tilde{\sigma}_{rr}\tilde{u}_r + \tilde{\sigma}_{r\theta}\tilde{u}_\theta)\cos\theta\right]\right\}\,d\theta \quad (4.5)$$

where $(\ )^{\cdot}$ denote differentiation with respect to θ. The values of I for five values of p and three values of n are tabulated in Table 1 for fields symmetric and anti-symmetric with respect to the crack plane.

We outline the solution procedure employed to determine the dependence of the stresses on θ. An Airy stress function is introduced and a partial differential equation governing the stress function is derived from the compatibility equation, the latter equation being written in terms of the stresses by using the constitutive relation (2.7). A separable form (see (4.1)) can be obtained thereby reducing the problem to a fourth order nonlinear ordinary differential equation with θ as the independent variable. A shooting method based on a combined fourth-fifth order Runge–Kutta scheme with error and step-size control is employed to generate the solution. Similar solution procedures have been employed by Shih (1973, 1974) and the details are given in Appendix I of the 1973 publication.

5. Mode I and Mode II singularity fields

To examine the effect of plastic orthotropy on the angular variation of the singularity fields, the dimensionless stresses $\tilde{\sigma}_e$ and $\tilde{\sigma}_{ij}$ and strains $\tilde{\epsilon}_{ij}$ are graphically presented for $p = 10, 2, 1, 0.5$ and 0.1, where $p = 0.5$ and 2 represent mildly orthotropic materials, and $p = 0.1$ and 10 represent highly orthotropic materials. The Mode I fields (symmetric with respect to the $x_2 = 0$ plane) are discussed first. Figs. 2 and 3 show the angular variations of $\tilde{\sigma}_e$, $\tilde{\sigma}_{rr}$, $\tilde{\sigma}_{\theta\theta}$, $\tilde{\sigma}_{r\theta}$ and $\tilde{\epsilon}_{rr}$ (note that

Table 1
Plane-strain values of I

p	Mode I			Mode II		
	$n = 3$	$n = 10$	$n = 20$	$n = 3$	$n = 10$	$n = 20$
10	4.23	3.09	2.89	1.93	1.54	1.47
2	5.63	4.27	3.90	1.28	0.97	0.90
1	5.51	4.54	4.21	0.95	0.74	0.69
0.5	4.96	4.42	4.22	0.69	0.55	0.52
0.1	4.10	4.04	4.03	0.33	0.27	0.25

The Mode II values of I (for $p = 1$) in Hutchinson's 1968b paper are incorrect. The correct values are given here and in Shih's 1974 paper.
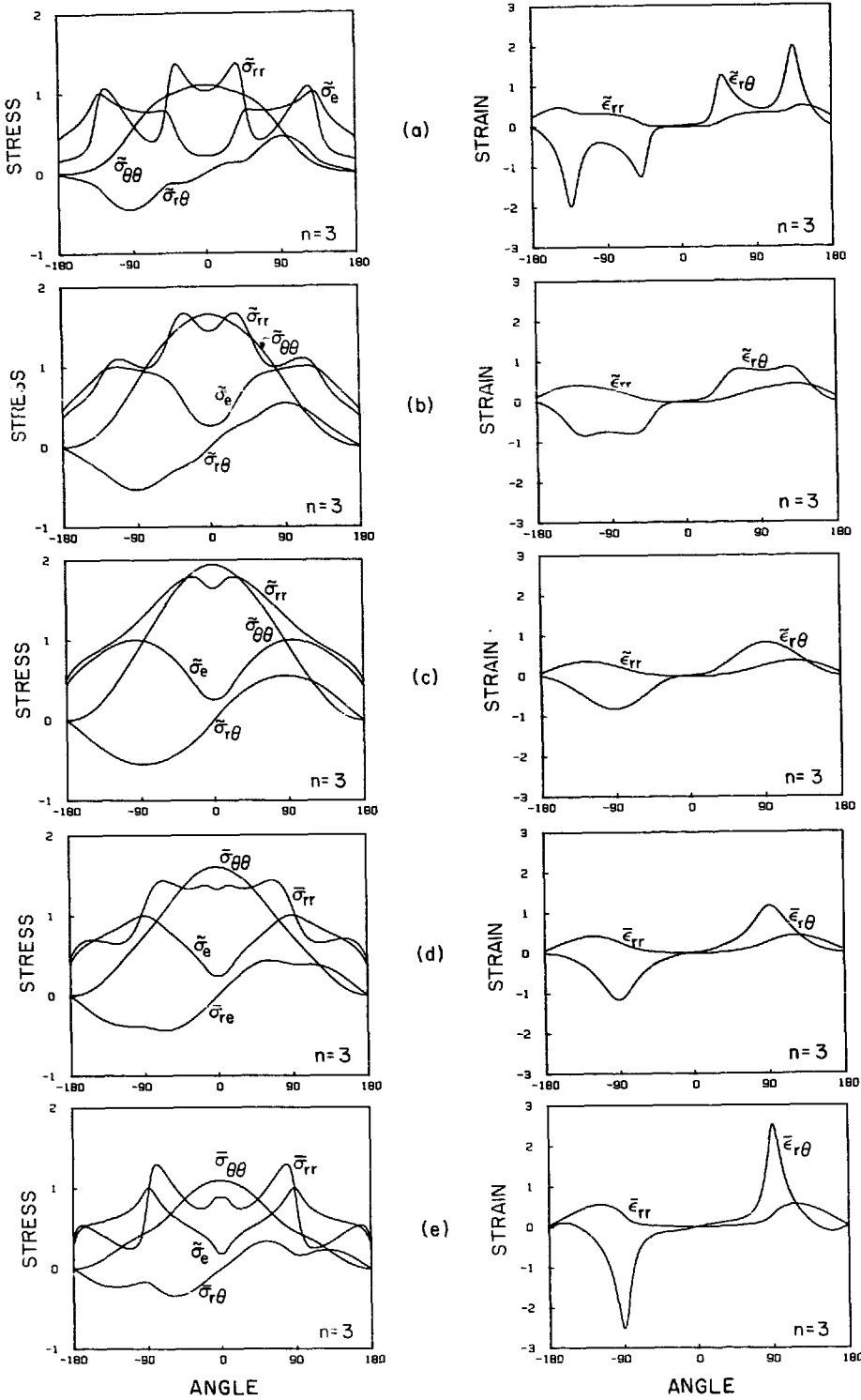
Fig. 2. Mode I angular distribution of normalized stresses and strains for $n = 3$: (a) $p = 10$, (b) $p = 2$, (c) $p = 1$, (d) $p = 0.5$, (e) $p = 0.1$.
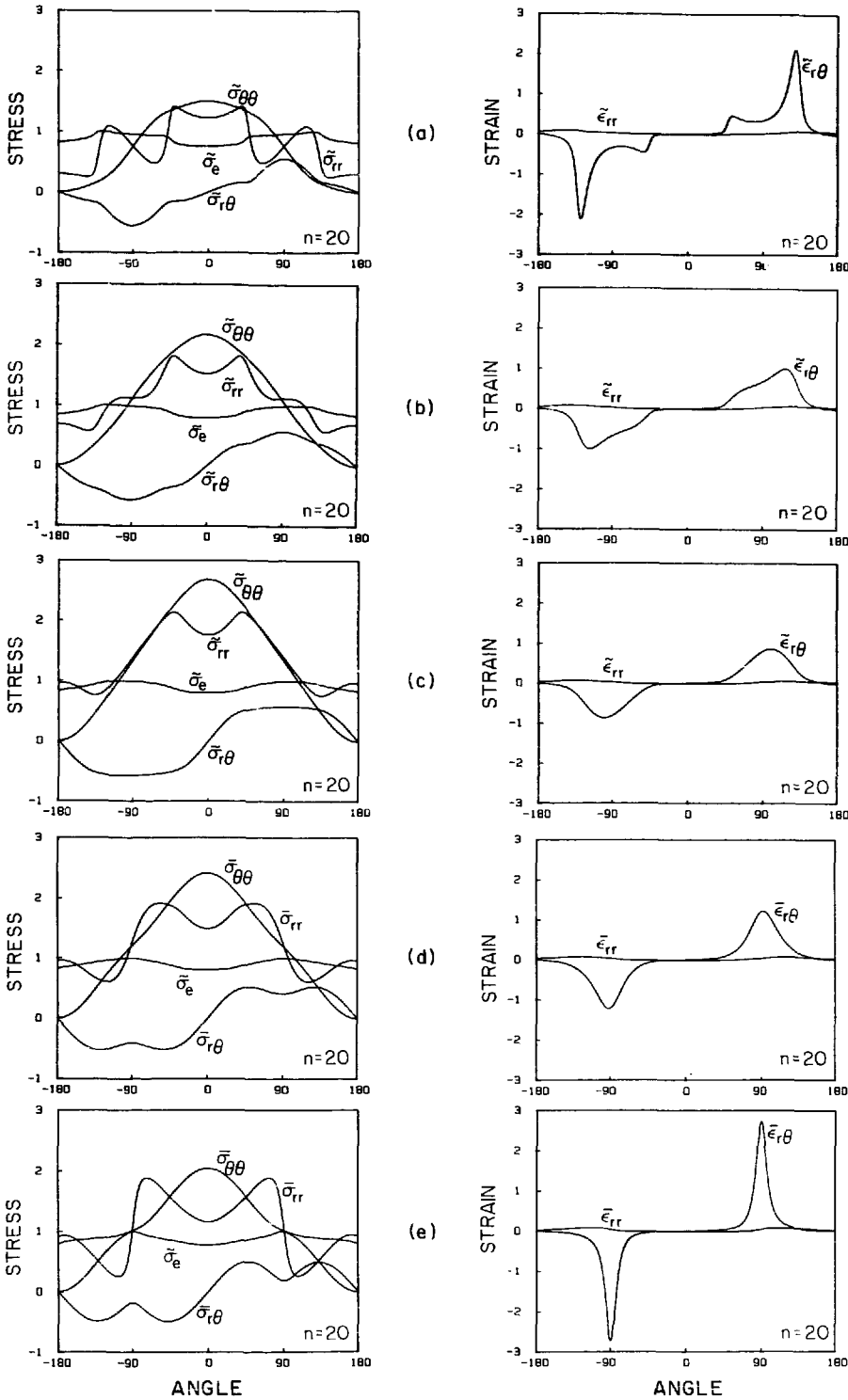
Fig. 3. Mode I angular distribution of normalized stresses and strains for $n = 20$: (a) $p = 10$, (b) $p = 2$, (c) $p = 1$, (d) $p = 0.5$, (e) $p = 0.1$.

$\bar{\epsilon}_{\theta\theta} = -\bar{\epsilon}_{rr}$) and $\bar{\epsilon}_{r\theta}$ for $n = 3$ and 20. The five cases are arranged in order of decreasing p values. The middle plot for $p = 1.0$ is precisely the angular distribution obtained by Hutchinson (1968a, b) and Rice and Rosengren (1968) for isotropic material. (We point out that fields identified by $p = 1$ are associated with isotropic materials as well as orthotropic materials with plastic properties such that $FG/(F + G) + H = \frac{1}{4}$).

Since the fields are symmetrical with respect to the x_1 axis, we will confine our attention to the interval $0° \leqslant \theta \leqslant 180°$. The effective stress $\bar{\sigma}_e$ for $p = 10$ and 2 falls off rather rapidly at $\theta < 45°$ and $\theta > 135°$ (see plots (a) and (b)). This behavior is more clearly seen in the strain plots where the shear strain $\bar{\epsilon}_{r\theta}$ peaks at θ of about 45° and 135°. For a low-hardening material, $n = 20$, the peak at 135° is the larger of the two peaks. For $p > 1$ the dimensionless stresses ahead of the crack are lower than the stresses for the $p = 1$ case. In subsequent discussions the angular distributions for $p > 1$, which include two zones of rapid variation of $\bar{\epsilon}_{r\theta}$, will be called type-B fields. For $p = 0.5$ and 0.1 it can be seen that $\bar{\sigma}_e$ peaks very rapidly at $\theta \cong 90°$. Again this behavior is more clearly revealed by the angular variation of $\bar{\epsilon}_{r\theta}$ in the strain plots. Our numerical calculations indicate that as p becomes increasingly small, the angular sector where $\bar{\epsilon}_{r\theta}$ is about unity becomes increasingly narrow. Furthermore the dimensionless stresses $\bar{\sigma}_{rr}$ and $\bar{\sigma}_{\theta\theta}$ are rather large. The possible implications of these fields on fracture toughness are discussed in Section 7. The normalized stresses in plots (d) and (e) have been scaled by $\sqrt{p}$, i.e., $\bar{\sigma}_{ij} = \sqrt{p}\,\bar{\sigma}_{ij}$. The strains in plots (d) and (e) are scaled by $1/\sqrt{p}$, i.e., $\bar{\epsilon}_{ij} = \bar{\epsilon}_{ij}/\sqrt{p}$. The rescaled strain plots reveal the trend that the shear strain peaks over an increasingly narrow angular sector as the value of p decreases from unity (note that the maximum value of $\bar{\epsilon}_{r\theta}$ is about unity for $p \leqslant 1$). The angular distributions for $p < 1$ will be called type-A fields.

For the purpose of explaining the angular distributions in Figs. 2 and 3, we consider a rather special orthotropic material with equal tensile yield stresses, i.e., $X = Y = Z$. The parameter p is then given by

$$p = 3(T/X)^2. \tag{5.1}$$

Thus $p < 1$ characterizes a material which yields more easily in shear (compared to the tensile yield stresses). As the shear yield stress becomes vanishingly small, $p \ll 1$, the behavior of the material becomes pathological and it is not surprising that the angular variation of the shear strain peaks very rapidly at $\theta \cong 90°$. At the other limit where the shear yield stress becomes infinitely large (compared to the tensile yield stresses), $p \gg 1$, the
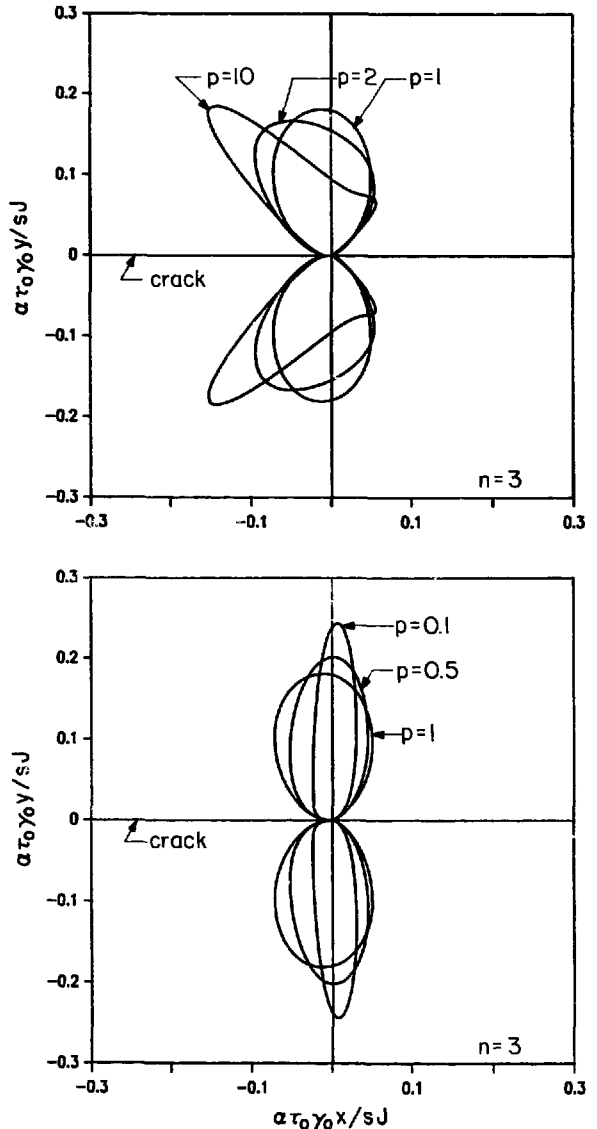

Fig. 4. Mode I effective stress contours for $n = 3$ plotted using similarity coordinates $(x, y)/[sJ/(\alpha\tau_0\gamma_0)]$: for $p = 10, 2, 1, 0.5$ and 0.1.

shear strain concentrates in the vicinity of $\theta \cong 45°$ and $135°$. We define a parameter β to be equal to $\sqrt{3}\,T/X$. For example, $\beta = 1$ represents an isotropic material, and β less/greater than 1 is the reduced/increased value of T from the isotropic value accorded by the J_2 theory of plasticity. With p defined by (5.1) we obtain the connection $\beta = \sqrt{p}$. Thus $p = 10$, 2, 1, 0.5 and 0.1 correspond to $\beta = 3.16$, 1.41, 1, 0.707, and 0.316, i.e., when $p = 0.1$, the shear yield stress of the orthotropic material is slightly less than a third of the isotropic value.

Of course the behavior noted above is not confined to material of nearly equal tensile yield stresses and relatively small shear yield stress. It is evident from (2.2) and (3.3) that a small value of p can result from a small value for T or the 'right' combination of the tensile yield stresses X, Y and Z. To make this point, we consider a material where the anisotropy is rotationally symmetrical about the principal axis X_3. Then

$$p = 4T^2\left(\frac{1}{X^2} - \frac{1}{4Z^2}\right).   (5.2)$$

Thus a small value of p can arise if T is small (relative to X and Z) or if X is nearly equal to $2Z$. Similarly p will assume a large value if T is large compared to X and Z.

The effective stress contours for the five cases are plotted in Fig. 4 for $n = 3$ and in Fig. 5 for $n = 20$ using the dimensionless similarity coordinates $(\alpha\tau_0\gamma_0/sJ)x$ and $(\alpha\tau_0\gamma_0/sJ)y$ where $s = (\tau_0/\tau_e)^{n+1}$. Contours for $p = 2$ and 10, or type-B fields, are drawn in Figs. 4(a) and 5(a); the contours for $p = 1$ are also included. The characteristics of the type-B fields can be seen. Contours for $p = 0.5$ and 0.1, or type-A fields, are plotted in Figs. 4(b) and 5(b). Here the shape of the contour becomes increasingly elongated as p becomes small and appear like narrow vertical strips above and below the crack tip for $p = 0.1$. If the singularity fields (4.1) are the full solution everywhere in the plastic zone, then the contours in Figs. 4 and 5 are the actual shapes of the elastic-plastic boundaries. Since (4.1) dominates over a region well within the plastic zone, these contours suggest a possible trend of the plastic zone size and shape as the degree of plastic orthotropy increases. Thus the
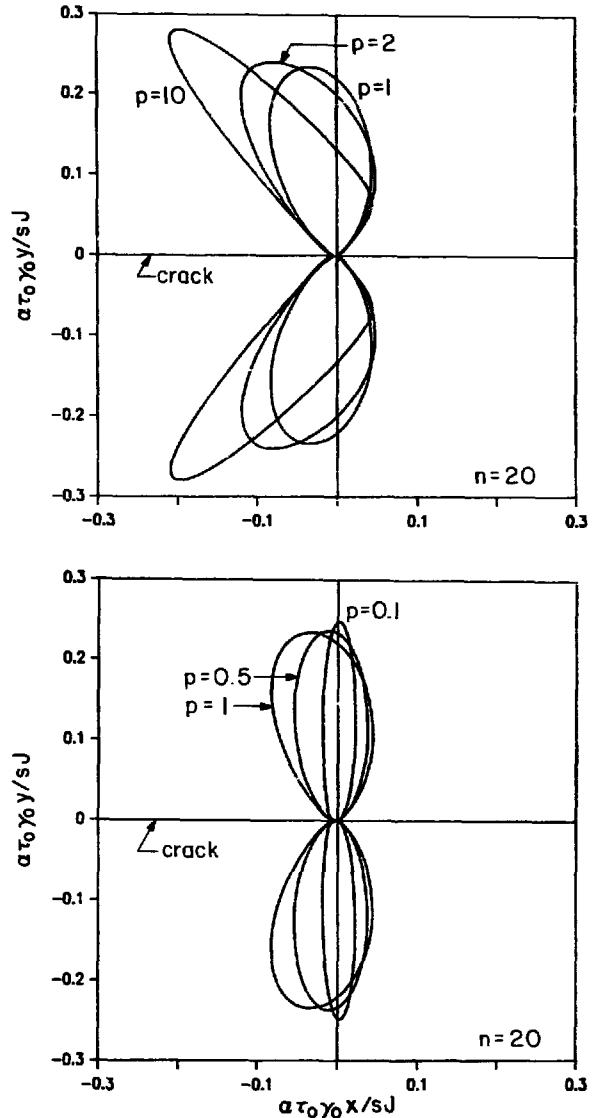

Fig. 5. Mode I effective stress contours for $n = 20$ plotted using similarity coordinates $(x, y)/[sJ/(\alpha\tau_0\gamma_0)]$ for $p = 10$, 2, 1, 0.5 and 0.1.

shape and size of the effective stress contours in Figs. 4 and 5 could be quite different from the actual elastic-plastic boundaries.

The angular variations of the stresses and strains corresponding to Mode II loading are shown in Figs. 6 and 7 for $n = 3$ and $n = 20$ respectively. Again the five cases are arranged in the order of decreasing p values. For $p > 1$, the shear strain peaks at $\theta \cong 45°$ and $135°$. The shear strain peak
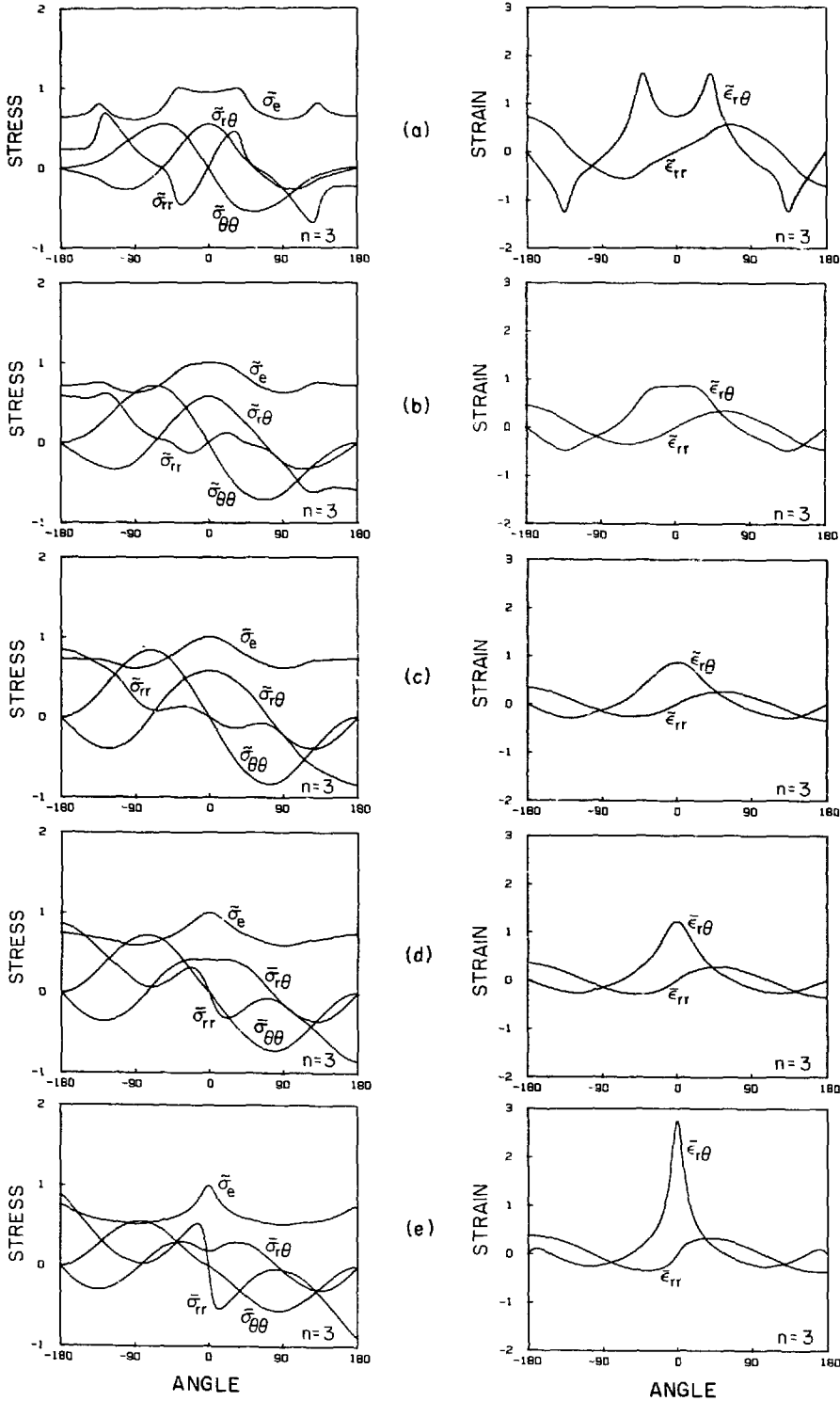
Fig. 6. Mode II angular distribution of normalized stresses and strains for $n = 3$: (a) $p = 10$, (b) $p = 2$, (c) $p = 1$, (d) $p = 0.5$, (e) $p = 0.1$.
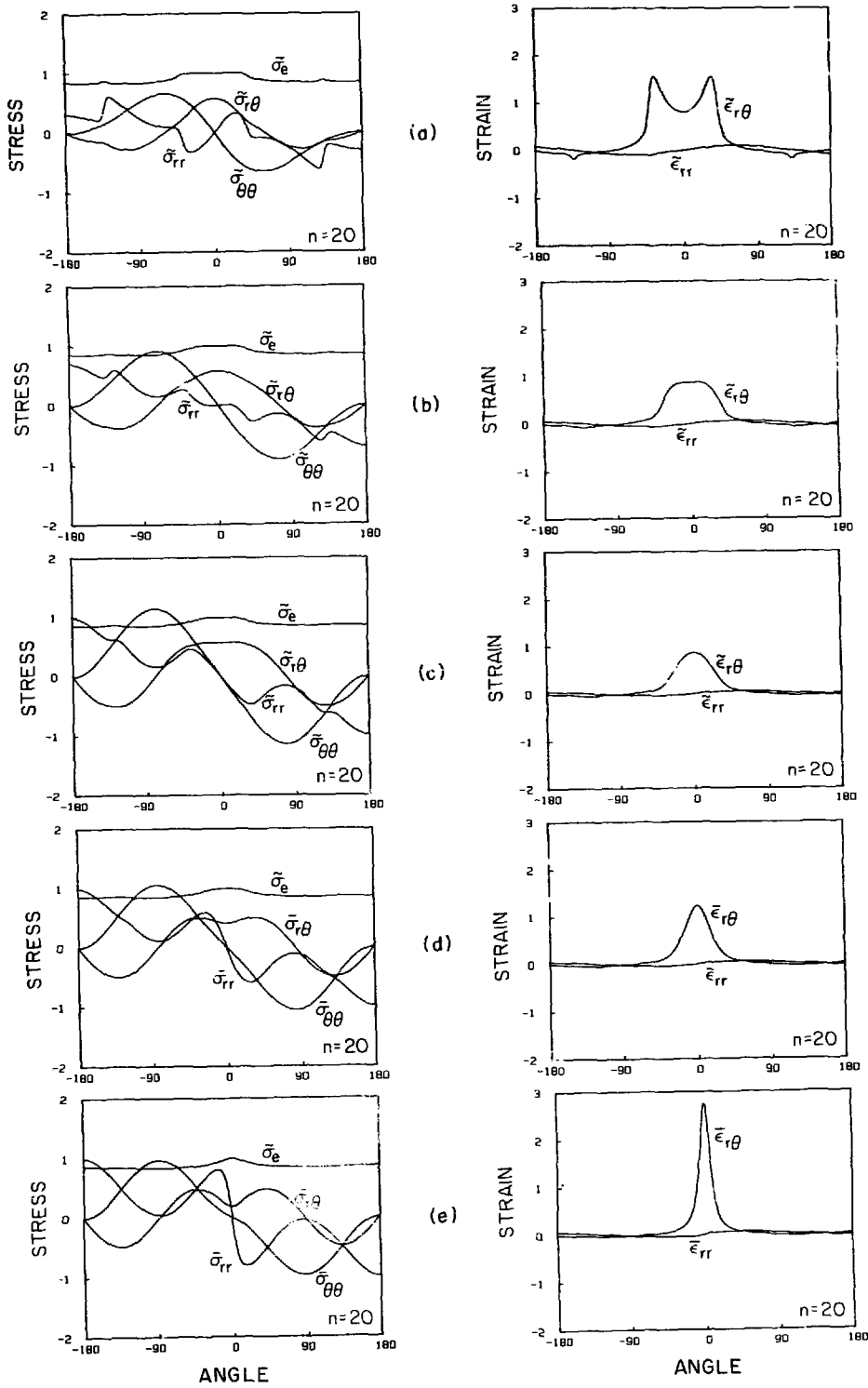
Fig. 7. Mode II angular distribution of normalized stresses and strains for $n = 20$: (a) $p = 10$, (b) $p = 2$, (c) $p = 1$, (d) $p = 0.5$, (e) $p = 0.1$.
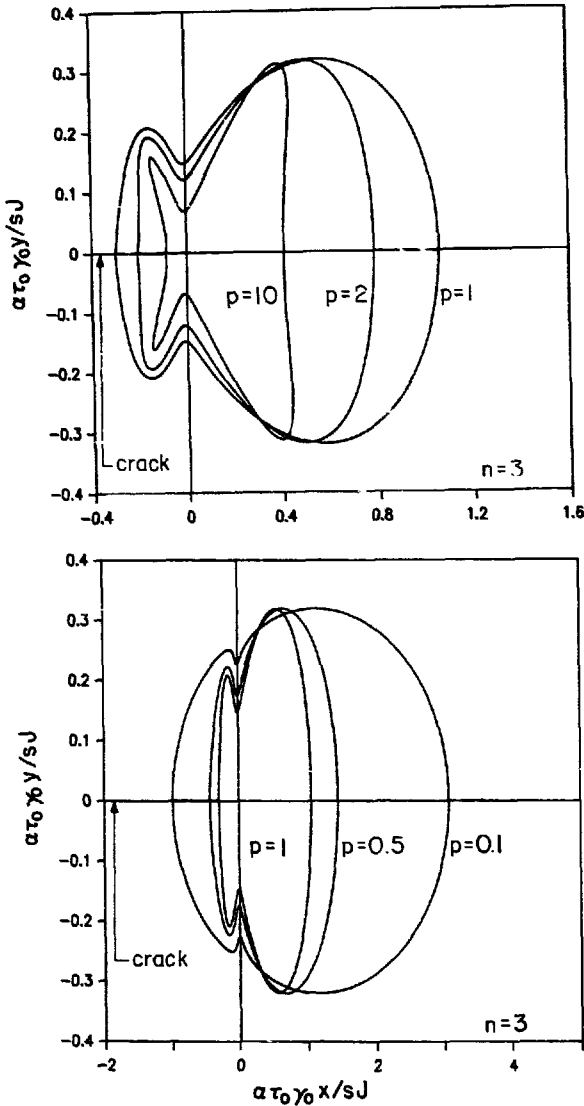
Fig. 8. Mode II effective stress contours for $n = 3$ plotted using similarity coordinates $(x, y)/[sJ/(\alpha\tau_0\gamma_0)]$: for $p = 10, 2, 1, 0.5$ and 0.1.
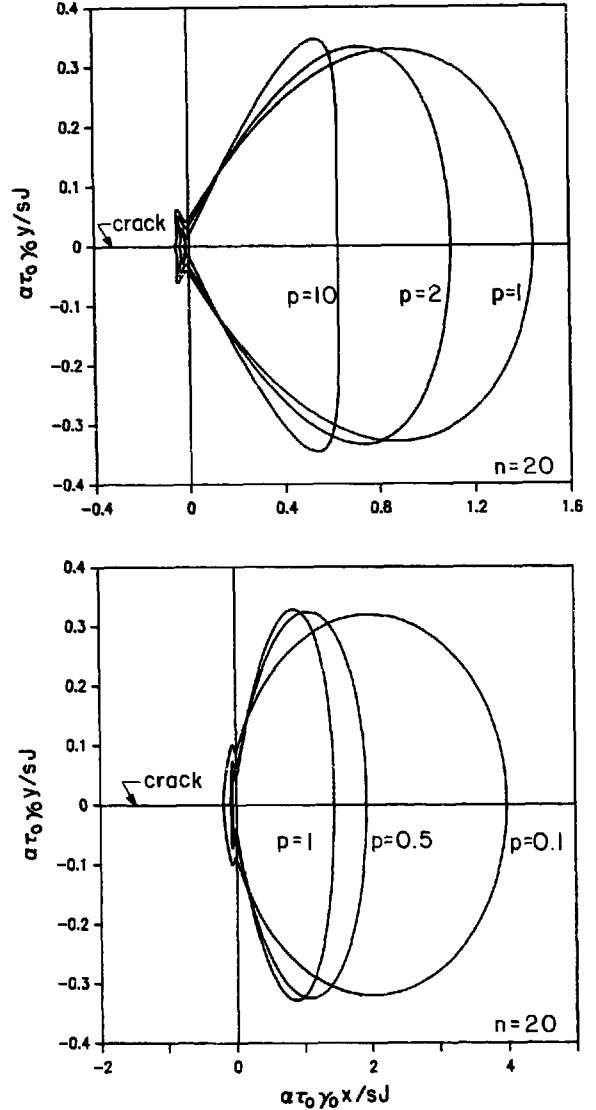
Fig. 9. Mode II effective stress contours for $n = 20$ plotted using similarity coordinates $(x, y)/[sJ/(\alpha\tau_0\gamma_0)]$: for $p = 10, 2, 1, 0.5$ and 0.1.

at $\theta \cong 45°$ is the dominant peak for the $n = 20$ material. As in the Mode I cases, angular distributions with two peaks ($p > 1$) will be called type-B fields. For $p < 1$, $\tilde{\epsilon}_{r\theta}$ peaks at $\theta = 0°$. The normalized stresses and strains in the plots (d) and (e) are defined by $\bar{\sigma}_{ij} = \sqrt{p}\,\tilde{\sigma}_{ij}$ and $\bar{\epsilon}_{ij} = \tilde{\epsilon}_{ij}/\sqrt{p}$. For $n = 20$ and $p = 0.1$ the shear strain distribution resembles a delta-function. Angular distributions for $p < 1$ will be called type-A fields. Effective stress

contours for the type-B and type-A fields are plotted in the similarity coordinates $(\alpha\tau_0\gamma_0/sJ)x$ and $(\alpha\tau_0\gamma_0/sJ)y$, where $s = (\tau_0/\tau_e)^{n+1}$, in Figs. 8 and 9 for $n = 3$ and 20 respectively; note that a different scale has been used for the ordinate. The characteristics of the type-B and type-A fields are clearly distinguishable in these plots. In particular, we call attention to the substantial increase of the radial distance (along the plane of the crack) of

the effective stress contour as the value of p decreases from unity.

6. Mode I and Mode II perfect plasticity solutions

A plane-strain slip-line theory for rigid/plastic incompressible materials with anisotropic convex yield surfaces has been developed by Rice (1973). Subsequently, Rice (1984) presented a general formulation of two-dimensional elastic-perfectly-plastic anti-plane straining for materials with arbitrary anisotropic convex yield surfaces and obtained anti-plane crack-tip slip-line fields under contained yielding. Based on the formulations in Rice (1982, 1984), crack-tip solutions for stationary and quasi-statically growing cracks in

Fig. 10. Mode I and II slip-line fields for perfectly-plastic orthotropic materials.

single crystals have been presented by Rice and Nikolic (1985). We use Rice's 1973 method to construct Mode I and Mode II plane-strain slip-line solutions for the ideally-plastic material with yield surface specified by (3.2). Details of the construction are given by Pan (1986) and will not be discussed here.

The Mode I plane-strain slip-line field for an orthotropic material is shown in Fig. 10(a). The included angles of the constant stress zones and the fan sectors are precisely equal to the angles for the Prandtl slip-line field for isotropic material. While the angular span of the various sectors do not depend on p, the stresses are strongly dependent on p. The left column of plots in Fig. 11 show the angular variations of σ_{rr}, $\sigma_{\theta\theta}$ and $\sigma_{r\theta}$ for the five cases $p = 10, 2, 1, 0.5$ and 0.1. In the plots (a), (b) and (c) the stresses have been normalized by the effective tensile yield stress σ_0, defined by $\sigma_0 = \sqrt{3}\,\tau_0$, where τ_0 is the effective shear yield stress (see (2.4)). The normalized stresses in plots (d) and (e), i.e. the type-A fields, have been scaled by $\sqrt{p}$, i.e. $\bar{\sigma}_{ij} = \sqrt{p}\,\sigma_{ij}/\sigma_0$. A comparison of the angular variations of the stresses in Fig. 3 with the Mode I stresses in Fig. 11 reveal remarkably close agreement between the low-hardening solution ($n = 20$) and the perfect plasticity solution. This close agreement strongly suggests that the non-hardening limit of the stresses of the dominant singularity solution is the perfect plasticity solution.

The Mode II slip-line field for an orthotropic material governed by (2.1) is shown in Fig. 10(b). The general features of the slip-line field are similar to those for the isotropic material. However the angular span of the fan sector directly ahead of the crack θ_1 increases/decreases as the value of p increases/decreases from unity; the angular span of the other two fan sectors θ_2 are determined from the condition $\theta_1 + 2\theta_2 = \frac{1}{2}\pi$. The right column of plots in Fig. 11 show the angular variations of the stresses for $p = 10, 2, 1, 0.5$ and 0.1. Again we note the remarkable resemblance between the stress distribution for the low-hardening material ($n = 20$) in Fig. 7 and the perfect plasticity solution.

The strains at the tip of the crack in perfect plasticity cannot be obtained by any elementary
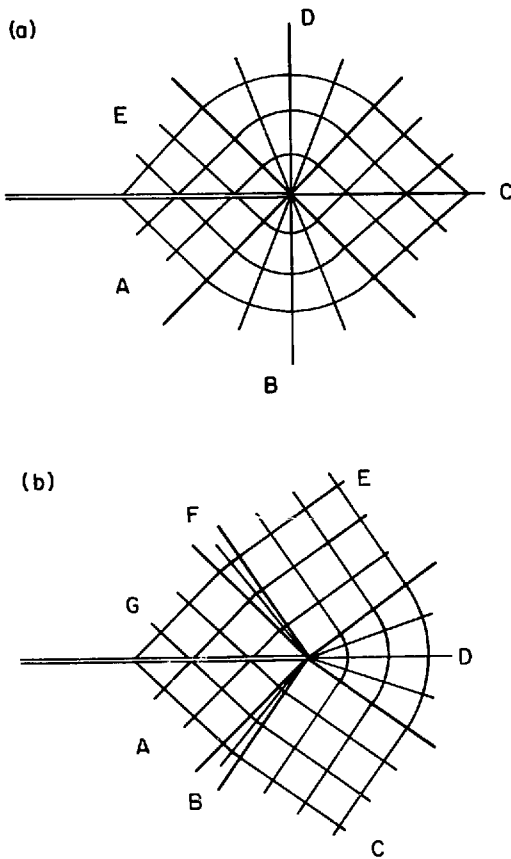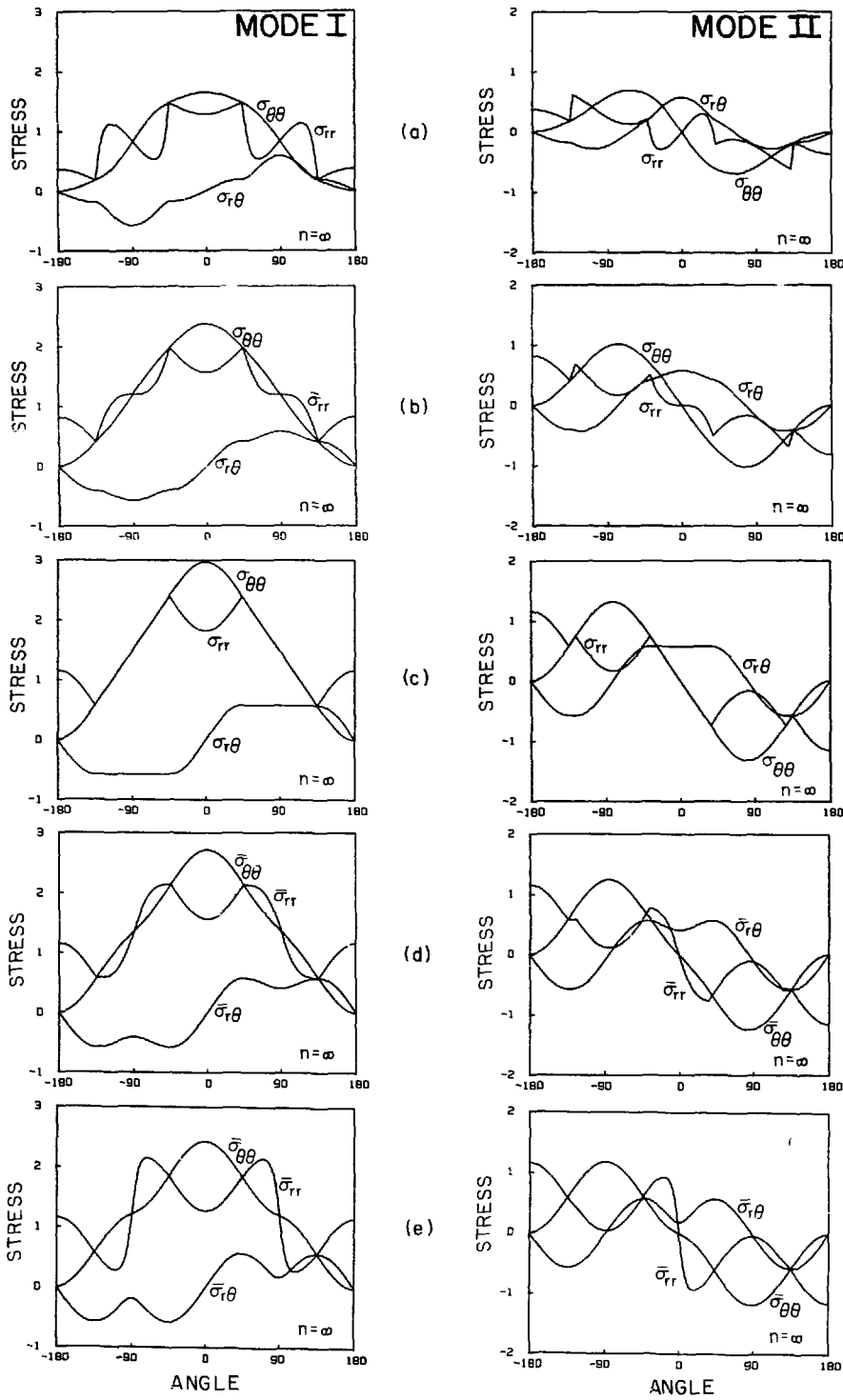
Fig. 11. Mode I and II stress distributions normalized by effective yield stress σ_0 for perfectly-plastic orthotropic materials: (a) $p = 10$, (b) $p = 2$, (c) $p = 1$, (d) $p = 0.5$, (e) $p = 0.1$.

analysis. However it may be noted that the $1/r$ singularity in strains can occur only in the fan sectors where the only non-zero component is $\epsilon_{r\theta}^P$. These features are reflected in the low-hardening strain fields of Figs. 3 and 7.

It is known that the solution near a stationary crack tip in perfectly plastic materials is not unique. Nemat-Nasser and Obata (1984) compare various solutions obtained for Mode I and II stress fields near a stationary crack tip on the basis of various assumptions. They show that, as far as the field equations are concerned, one may admit solutions with elastic sectors. They conclude, however, that Prandtl's solution seems most reasonable for Mode I. Also, they conclude that, for Mode II, Hutchinson's solution (1968b) is one out of other possibilities and that, in this case, a solution with elastic sector may be more reasonable, by considering a limiting case of the dynamic solution. Nevertheless, Hutchinson (1968b) and Shih (1983) show that the stresses of Hutchinson's Mode II solution (with no elastic sector) agree with the stresses of the nonhardening limit of the corresponding power-law solutions. Our numerical investigations strongly indicate that the nonhardening limit of the stresses of our power-law hardening solutions for anisotropic materials is our slip-line solution. Our slip-line solutions, however, do not contain any elastic sectors. Nemat-Nasser and Obata (1984) also show that by allowing the existence of elastic sectors, one obtains continuous stress field for mixed Mode I and II, whereas the solutions by Shih (1974), guided by the nonhardening limit of the power-law hardening solutions, contain no elastic sector and have radial stress discontinuity when Mode I loading is dominant.

For a power-law material, Gao and Nemat-Nasser (1983) obtained a dynamic solution which involves no elastic unloading for Mode I. The angular distribution is the same as that for elastic perfectly plastic case: i.e., no elastic unloading, whereas the corresponding quasi-static solution involves an elastic unloading sector (see Rice (1982) for many references on this subject). For the Mode II solution, Gao and Nemat-Nasser (1983) obtained elastic unloading close to the crack surfaces; the quasi-static solution for elastic per-

fectly plastic case also involves elastic unloading but at different locations. For the mixed Mode I and II dynamic cases, Nemat-Nasser (1986) indicates that the presence of any amount of Mode I loading dominates the stress field and may completely eliminate the elastic sector.

7. Discussion

Thus far we have confined the discussion to the case where the material X_1-axis coincides with the x_1-axis. By the results of Section 3, p remains unchanged when the X_1-axis is rotated from the x_1-axis by $\frac{1}{2}m\pi$ ($m = 1, 2, 3$); furthermore, the symmetric angular distributions in Figs. 2, 3 and 11(a) and the anti-symmetric angular distributions in Figs. 6, 7 and 11(b) are also unchanged, and the values of I in Table 1 are preserved. For discussion purposes we refer to these as group-0 fields. Suppose that the X_1-axis is rotated from the x_1-axis by $\frac{1}{4}\pi + \frac{1}{2}m\pi$ ($m = 0, 1, 2, 3$). By the results of Section 3, x_1, x_2 and x_3 remain axes of symmetry and the angular variations of the near-tip fields do not depend on m; these fields are referred to as group-45 fields. For the purpose of making the connection between group-0 and group-45 fields, the yield criterion (2.4) is specialized to plane-strain conditions and restated in the form

$$\hat{\tau}_e^2 = \tfrac{1}{4}\hat{p}(\sigma_{11} - \sigma_{22})^2 + \sigma_{12}^2 = \hat{T}^2. \tag{7.1}$$

Group-0 fields are associated with (3.2) whereupon we make the identifications

$$\hat{\tau}_e = \tau_e, \qquad \hat{T} = T, \qquad \hat{p} = p. \tag{7.2}$$

Group-45 fields are associated with (3.8) whereupon these identifications are made

$$\hat{\tau}_e = \frac{\tau_e}{\sqrt{p}}, \qquad \hat{T} = \frac{T}{\sqrt{p}}, \qquad \hat{p} = \frac{1}{p}. \tag{7.3}$$

Thus group-0 angular distributions for $p = 10, 2, 1, 0.5$ and 0.1 as shown in Figs. 2, 3, 6, 7 and 11 are identical to group-45 angular distributions for $p = 0.1, 0.5, 1, 2$ and 10. In other words, while group-0 type-A fields are characterized by $p < 1$, group-45 type-A fields are characterized by $p > 1$. Group-0 and group-45 type-B fields are char-

acterized by $p > 1$ and $p < 1$ respectively. Similarly the value of the integration constant for the group-45 fields, $I_{45}(n, p)$ is equal to $I(n, 1/p)$. It also follows from (7.3) that the form of the group-45 near-tip fields is still given by (4.1) with I_{45} replacing I and $\tau_0/\sqrt{p}$ and $\gamma_0/\sqrt{p}$ replacing τ_0 and γ_0 respectively.

If the orientations of the axes of orthotropy do not fall into any of the two groups under discussion, the fields in general do not possess the symmetries (Mode I or Mode II) discussed. In other words remote tensile stress or remote shear stress will induce near-tip fields whose angular variations are neither symmetric nor anti-symmetric. These fields will depend implicitly on an additional parameter which measures the angular separation of the material X_1-axis from the crack plane (or the x_1-axis). Mixed-mode near-tip fields for plastically deforming isotropic materials have been discussed by Shih (1973, 1974).

It can be seen from Figs. 2 and 3 that the dimensionless Mode I stresses $\tilde{\sigma}_{\theta\theta}$ and $\tilde{\sigma}_{rr}$ are substantially elevated above $\tilde{\sigma}_e$ (or $\tilde{\tau}_e$) as the value of p decreases from unity (note that $\bar{\sigma}_{ij} = \sqrt{p}\,\tilde{\sigma}_{ij}$). These distributions indicate that the (tensile) hoop and radial stresses (and the hydrostatic stress) will be substantially elevated above the effective shear/tensile yield stress defined by (2.4) for $p < 1$. To gauge this effect of orthotropic plasticity we consider materials whose response under shear with respect to the X_1-X_2-axes can be described by the identical shear strain–shear stress relation. However, these materials respond differently under tensile stressing along the principal axes. For example the materials under consideration will have the same α, τ_0, γ_0 and n values if their behavior can be represented by the Ramberg–Osgood relation (2.6). At a fixed radial distance r from the crack tip, and for the same value of J, the stresses and strains at the near-tip regions of these various materials vary as

$$\sigma_{ij} \propto \tilde{\sigma}_{ij}(\theta) I^{-1/(n+1)},$$

$$\epsilon_{ij} \propto \tilde{\epsilon}_{ij}(\theta) I^{-n/(n+1)} \qquad (7.4)$$

where it has been noted that the dimensionless angular functions $\tilde{\sigma}_{ij}$ and $\tilde{\epsilon}_{ij}$ and the constant I depend implicitly on n and p. Using the values of

I in Table 1 and $\tilde{\sigma}_{ij}$ in Figs. 2 and 3, it can be easily checked that for $p = 0.1$ and $n = 20$ the tensile stresses are at least a factor of two larger than the corresponding values for $p = 1.0$.

The tensile hoop stress $\sigma_{\theta\theta}$ ahead of the crack ($\theta = 0$) appears to have an important role in fracture initiation. Within the zone dominated by (4.1), the ratio of the tensile stress for the $p \neq 1$ material to that for the $p = 1$ material is

$$\frac{\sigma_{\theta\theta}(p \neq 1)}{\sigma_{\theta\theta}(p = 1)} = \frac{\tilde{\sigma}_{\theta\theta}(p \neq 1)}{\tilde{\sigma}_{\theta\theta}(p = 1)} \left[\frac{I(p = 1)}{I(p \neq 1)} \right]^{1/(n+1)}, \qquad (7.5)$$

This ratio for Mode I is plotted in Fig. 12 as a function of p for $n = 3, 10, 20$ and ∞; the $n = \infty$ curve is obtained from the perfect plasticity analysis. The elevation of the tensile stress above the isotropic value for $p < 1$ is very large for the low-hardening material. The hydrostatic stress behaves in a similar manner. This elevation of the tensile stresses warrants attention since experiments and model calculations have shown that high tensile and hydrostatic stresses are detrimental to fracture toughness.

The ratio of the peak strains (within the zone dominated by (4.1)) can be expressed by a similar
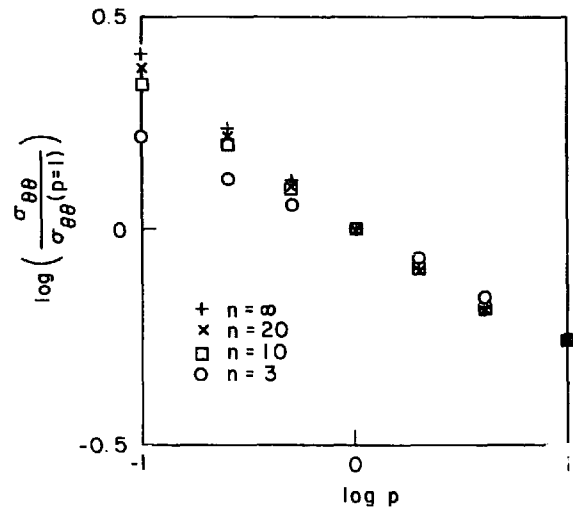

Fig. 12. Ratio of Mode I hoop stress ahead of the crack in an orthotropic material to hoop stress in an isotropic material for $n = 3, 10, 20$ and ∞.

relation, e.g., the shear strain ratio is given by

$$\frac{\epsilon_{r\theta}(p \neq 1)}{\epsilon_{r\theta}(p=1)} = \frac{\tilde{\epsilon}_{r\theta}(p \neq 1)}{\tilde{\epsilon}_{r\theta}(p=1)} \left[\frac{I(p=1)}{I(p \neq 1)} \right]^{n/(n+1)}$$

(7.6)

Using the Mode I $\tilde{\epsilon}_{r\theta}$ from Figs. 2 and 3 and the I values of Table 1 in (7.6), it is apparent that the shear strain ratio is larger than unity for $p > 1.0$. It may be noted that plastic deformation within the near-tip region of highly orthotropic materials (as characterized by $p \ll 1$ or $p \gg 1$) consists primarily of intense shear emanating from the crack tip along certain orientations (see Figs. 2, 3, 6, and 7). Such intense deformation patterns could be favorable to the development of localized shear bands.

We also want to draw attention to another aspect of the near-tip fields. At the same value of J the magnitude of the near-tip stresses due to Mode I loading is larger than the magnitude of stresses caused by Mode II loading on the identical cracked body. The difference is very substantial for the low hardening material ($n = 20$). This is an effect of plasticity since the difference between Mode I and II stress magnitudes is negligible for the elastic body ($n = 1$). On the other hand, the near-tip strain magnitude under Mode II loading is much larger than that under Mode I loading especially at small values of p. This can be easily checked by using the tabulated I values for Mode I and II (in Table 1), the angular functions in Figs. 2, 3, 6 and 7 and equation (7.4).

We have discussed at some length plane-strain near-tip fields for a wide range of p values. Many engineering materials have deformation characteristics which may be broadly characterized as orthotropic, e.g., highly textured crystalline materials and composites. Consider a fiber reinforced composite with fibers aligned in the x_2-direction and suppose that the nonlinear macroscopic deformation characteristics of the composite can be approximated by the orthotropic plasticity model of Section 2. The composite has a crack oriented along the x_1-direction. Suppose the crack length and the size of the plane-strain region are large compared to the fiber diameter and spacing, and that the plastic zone size is of the order of ten

fiber spacings or more. We can then expect (4.1) to be an adequate representation of the macroscopic fields within the plastic zone. These outer macroscopic fields could presumably set the boundary conditions for a more precise model of the crack-tip region which takes into account the heterogeneity at the scale of fiber spacings. The viability of such an approach remains to be investigated. We also point out that under plane-strain conditions, the orthotropic plasticity formulation adopted in this study predicts no difference in the angular distribution of the macroscopic stresses and plastic strains between two limiting cases: the crack parallel to many fibers and the crack cutting across (perpendicular to) many fibers. Nevertheless on the scale of fiber spacing, the stresses and strains will depend on the orientation of the crack relative to the fibers.

Small scale yielding analysis based on a piecewise-power law representation of material behavior and generalized by Hill's yield criterion (2.1) is being carried out by Barsoum (1985). The incremental plasticity plane-strain finite element calculations employed a rather refined near-tip mesh which can accommodate the high stress and strain gradients expected at the crack tip; the pertinent plasticity parameters are $n = 3$ and $p = 0.1$, and the strong material axis is perpendicular to the crack plane. Barsoum finds that the plastic zone is more elongated than the corresponding plastic zone for an isotropic material and that the elastic-plastic boundary for the orthotropic material is quite similar to the contour for $p = 0.1$ in Fig. 4. The angular variations of the stresses and strains computed at Gauss points well within the plastic zone are similar to the distributions shown in Fig. 2. Nevertheless he observes that the details of the stress and strain distributions ahead $(0° \leqslant \theta \leqslant 30°)$ and behind $(150° < \theta \leqslant 180°)$ the crack differed somewhat from the singularity fields. The discrepancy is not surprising since, for highly orthotropic material, the extent of the plastic zone ahead and behind the crack tip is rather small compared to the overall size of the plastic zone (these features are indeed suggested by Figs. 4 and 5). In the zones in question the Gauss points are relatively close to the elastic-plastic boundary. In other words the Gauss points could be too

remote from the zone dominated by the singularity fields to be suitable for detecting the details of the singularity fields. Since the failure processes are generally activated in a region ahead of the crack tip, the detailed distributions of the stresses and strains ahead of the crack tip deserve further investigation.

Under small scale yielding and for isotropic elasticity J and the elastic stress intensity factor K_I are related by

$$J = \frac{(1 - \nu^2)}{E} K_I^2 \qquad (7.7)$$

For orthotropic elasticity, a similar relation between K_I and J can be derived using the elasticity solutions catalogued by Sih and Chen (1981) and Irwin's crack closure procedure for the energy release rate. The value of J can also be determined directly using strength of material type analysis and energy procedures. Such procedures have been discussed by Rice (1968a, b), Rice, Paris and Merkle (1973), and have been reviewed in recent literature (e.g., Kanninen and Popelar, 1985).

Acknowledgement

References

Barsoum, R. (1985), "Small-scale yielding plane-strain analysis of cracked orthotropic plates", work in progress.

Hayashi, K. (1979), "Singular behavior at the tip of a crack in an elastic-plastic material with plastic orthotropy", *J. Mech. Phys. Solids 27*, 163.

Gao, Y.C. and S. Nemat-Nasser (1983), "Near-tip dynamic fields for a crack advancing in a power-law elastic-plastic material: Mode I, II, and III", *Mechanics of Materials 2*, 305.

Hill, R. (1948), "A theory of the yielding and plastic flow of anisotropic metals", *Proc. Roy. Soc. London, Ser. A. 193*, 281.

Hill, R. (1950), *The Mathematical Theory of Plasticity*, Oxford University Press, London,

Hill, R. (1979), "Theoretical Plasticity of Textured Aggregates", *Math. Proc. Camb. Phil. Soc. 85*, 179.

Hutchinson, J.W. (1968a), "Singular behaviour at the end of a tensile crack in hardening materials", *J. Mech. Phys. Solids 16*, 13.

Hutchinson, J.W. (1968b), "Plastic stress and strain fields at a crack tip", *J. Mech. Phys. Solids 16*, 337.

Hutchinson, J.W. (1983), "Fundamentals of the phenomenological theory of nonlinear fracture mechanics", *J. Appl. Mech. Trans. ASME 50*, 1042.

Kanninen, M.F. and C.H. Popelar (1985), *Advanced Fracture Mechanics*, Oxford University Press, London.

Nemat-Nasser, S. and M. Obata (1984), "On stress fields near a stationary crack-tip", *Mechanics of Materials 3*, 235.

Nemat-Nasser, S. (1986), unpublished research.

Pan, J. (1986), "Plane-strain crack-tip stress for anisotropic perfectly plastic materials", *J. Mech. Phys. Solids 34*, 617.

Rice, J.R. and G.F. Rosengren (1968), "Plane strain deformation near a crack tip in a power-law hardening material", *J. Mech. Phys. Solids 16*, 1.

Rice, J.R. (1968a), "A path-independent integral and the approximate analysis of strain concentration by notches and cracks", *J. Appl. Mech. Trans. ASME 35*, 379.

Rice, J.R. (1968b), "Mathematical analysis in the mechanics of fracture", in: H. Liebowitz, ed., *Fracture, Vol. 2*, Academic Press, New York, 191.

Rice, J.R. (1973), "Plane strain slip line theory for anisotropic rigid/plastic materials", *J. Mech. Phys. Solids 21*, 63.

Rice, J.R. (1982), "Elastic-plastic crack growth," in: H.G. Hopkins and M.J. Sewell, eds., *Mechanics of Solids: The Rodney Hill 60th Anniversary Volume*, Pergamon Press, Oxford/New York, 539.

Rice, J.R. (1984), "On the theory of perfectly plastic anti-plane straining", *Mechanics of Materials 3*, 55.

Rice, J.R., P.C. Paris and J.G. Merkle (1973), "Some further results on *J*-integral analysis and estimates", in: Progress in Flaw Growth and Fracture Toughness Testing, ASTM STP 536, P. 231.

Rice, J.R. and R. Nikolic (1985), "Anit-plane shear crack in ideally plastic crystals", *J. Mech. Phys. Solids 33*, 595.

Shih, C.F. (1973), "Elastic-plastic analysis of combined mode crack problems", Ph.D. Thesis, Harvard Univ., Cambridge, MA.

Shih, C.F. (1974), "Small-scale yielding analysis of mixed mode plane-strain crack problems", Fracture Analysis, ASTM STP 560, American Society for Testing and Materials, 187.

Shih, C.F. (1983), "Tables of Hutchinson–Rice–Rosengren singular field quantities", MRL E-147, Materials Research Laboratory, Brown University.

Sih, G.C. and E.P. Chen (1981), *Cracks in Composite Materials*, Martinus Nijhoff, The Hague.